

Water Resources Research

RESEARCH ARTICLE

10.1029/2023WR036914

Key Points:

- We revealed the feedback mechanism between bank retreat and debris flow erosion efficiency
- We established a parameterized model describing the bank retreat process
- We discussed the relationships between the model parameters and the particle size distribution of the bank soil

Correspondence to:

J. Chen, chenjg@imde.ac.cn

Citation:

Wang, X., Chen, J., Chen, X., Chen, H., Zhao, W., Ruan, H., & Wang, J. (2024). Bank retreat mechanisms driven by debris flow surges: A parameterized model based on the results of physical experiments. *Water Resources Research*, 60, e2023WR036914. https://doi.org/10.1029/2023WR036914

Received 18 DEC 2023 Accepted 11 JUL 2024

© 2024. The Author(s). This is an open access article under the terms of the Creative Commons Attribution License, which permits use, distribution and reproduction in any medium, provided the original work is properly cited.

Bank Retreat Mechanisms Driven by Debris Flow Surges: A Parameterized Model Based on the Results of Physical Experiments

Xi'an Wang^{1,2} , Jiangang Chen^{1,2,3} , Xiaoqing Chen^{1,2} , Huayong Chen^{1,2}, Wanyu Zhao^{1,2,3}, Hechun Ruan^{1,2}, and Jinshui Wang^{1,2}

¹State Key Laboratory of Mountain Hazards and Engineering Resilience, Institute of Mountain Hazards and Environment, Chinese Academy of Sciences, Chengdu, China, ²University of Chinese Academy Sciences, Beijing, China, ³Sichuan Engineering and Technology Center for Mountain Hazard, Chengdu, China

Abstract Lateral erosion is a critical factor that influences the formation and amplification of debris flows. However, our understanding of the bank retreat process in debris flow channels is limited, which limits the evaluation of debris flow magnitudes and the prediction of their activity trends. Herein, we conduct physical experiments to investigate bank retreat mechanisms using five types of bank soil and multiple debris flow surges. The bank retreat process is categorized into two stages: toe cutting and bank collapse. Toe cutting is mainly caused by hydraulic erosion, bank collapse includes gravity erosion in the form of toppling failure. Notably, the bank retreat process exhibits a significant negative feedback loop. Bank erosion widens the channel bed, subsequently decreasing the flow depth. In turn, this reduction in flow depth mitigates bank erosion. Moreover, we discover a concise pattern in the complex coupling of hydraulic erosion and toppling failure: erosion efficiency is linearly and negatively correlated with the bed widening width. We develop a new parameterized model for describing the bank retreat process and provided empirical values for the model parameters. Furthermore, we observe that the initial erosion efficiency first increases and then decreases with an increase in the fine particle content of the bank soil. Additionally, we report a negative correlation between the maximum bed widening width and the fine particle content in the bank soil that follows a power function relationship.

1. Introduction

Debris flows are typically composed of water, poorly sorted sediment, wood, and other substances (Chen et al., 2021; Iverson, 1997; Lancaster et al., 2003; Takahashi, 2007), and they usually exhibit multiple surges within a single event (Chen et al., 2011; Huebl & Kaitna, 2021; Imaizumi et al., 2019; Kean et al., 2013; Zanuttigh & Lamberti, 2007). Furthermore, debris flows typically exhibit high sediment contents (Church & Jakob, 2020; Iverson, 1997; Pudasaini & Mergili, 2019), which implies the occurrence of extensive erosion and sedimentation in the upstream and downstream areas of debris gullies, thereby resulting in severe disasters (Cui et al., 2013; Garcia-Martinez & Lopez, 2005; Hu et al., 2012; Mergili et al., 2020; Pudasaini & Fischer, 2020). To gain a comprehensive understanding and to thoroughly evaluate the initiation and scale amplification processes of debris flows, various specific erosion theories have been established and developed (Iverson, 2012; Pudasaini & Krautblatter, 2021; Takahashi, 2007). Iverson (2012) considered factors such as the distribution of pore water pressure and debris flow velocity at flow depths that influence erosion. Moreover, fully mechanical erosion models have been established to account for the interactions between multiphase materials within debris flows (Pudasaini & Fischer, 2020; Pudasaini & Krautblatter, 2021; Pudasaini & Mergili, 2019). Recent studies have been increasingly focused on the contribution of collision stress in debris flow erosion (de Haas and Woerkom, 2016; Song & Choi, 2021). These erosion theories primarily concern channel bed erosion, emphasizing the hydraulic erosion process, which involves direct erosion caused by the forces from debris flows. However, channel bank erosion, which involves the coupling of hydraulic erosion and gravity erosion (Lyu et al., 2017; Zhou et al., 2015), differs significantly from channel bed erosion.

Gully bank erosion provides an important material supply for debris flows. Field investigations have shown that the material supply from gully banks is a significant factor influencing the formation and scale amplification of debris flows (Cui et al., 2013; Imaizumi et al., 2019; Lyu et al., 2022). Physical model experiments have demonstrated the substantial impact of bank erosion on increasing the magnitude and velocity of a debris flow

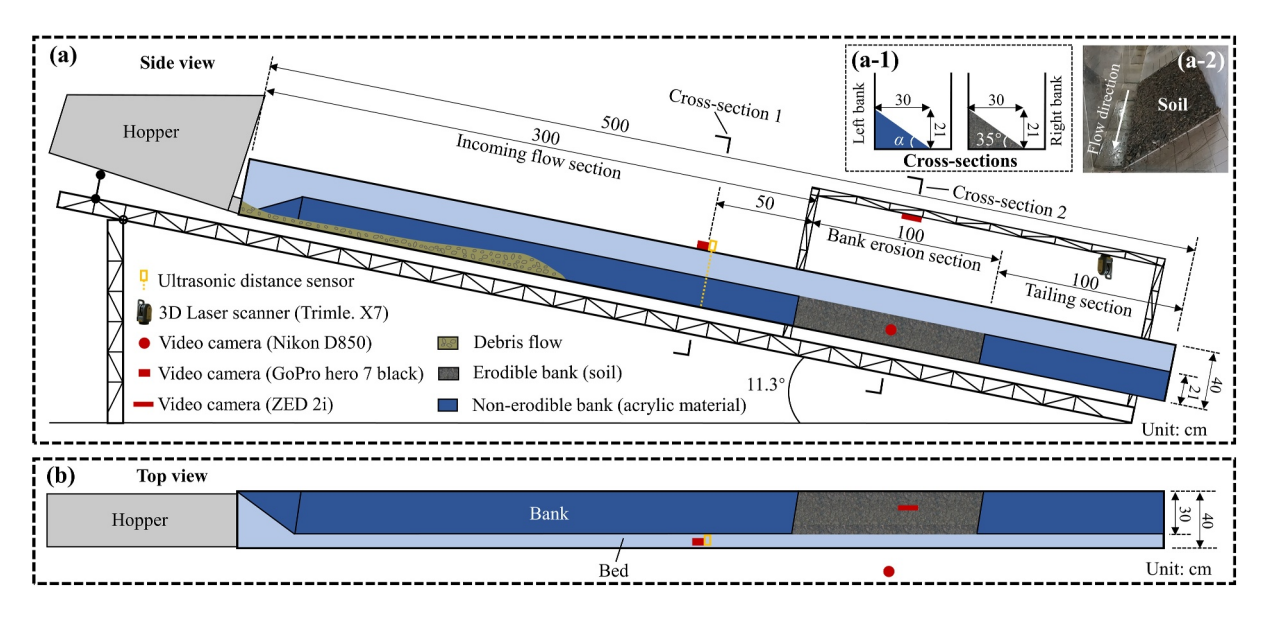


Figure 1. Experimental setup. (a) Schematic diagram of the side view (a-1) flume cross-sections (a-2) picture of the bank soils; and (b) schematic diagram of the top view

(Lyu et al., 2017; Zhou et al., 2015). Common sources of gully bank materials include landslide and collapse deposits, slope deposits, and alluvial fans from branch gullies (Berger et al., 2011; Imaizumi et al., 2019; Schwab et al., 2008). Erodible gully banks often have slopes and are not continuous throughout the channel, with some sections lacking erodible soils (Cui et al., 2013; Lyu et al., 2022; Zhou et al., 2015). In engineering applications, the material supply effect of bank erosion on a debris flow is considered in the form of a generalized blockage amplification coefficient (Chen et al., 2012; Cui et al., 2011, 2023; Ouyang et al., 2019), which is usually influenced by factors such as channel topography (degree of blockage), soil particle composition, length of erodible sections, and rainfall intensity (Chen et al., 2012; Cui et al., 2011; Ouyang et al., 2019).

Lateral erosion not only serves as a material source for debris flows but also profoundly influences channel topography, particularly by widening the channel (Fan et al., 2018; Zhang & Zhang, 2017). Concurrently, the widening of the channel is followed by a decrease in debris flow density (Zhou et al., 2015). This sequence of events prompts an intriguing question: How to quantify the feedback relationship between gully bank retreat and the lateral erosion efficiency of debris flows? However, this interesting aspect has been overlooked in prior physical model experiments that predominantly concentrated on the impacts of bank erosion on the formation, pattern, and discharge of debris flows (Lyu et al., 2017; Zhou et al., 2015), as well as the influence of debris flow density on bank erosion volume (Zhang et al., 2023). Investigating the process of bank retreat and its impact on the lateral erosion efficiency of debris flows through physical model experiments can enhance our understanding of the evolution of gully bank erosion and the activity trends of debris flows.

The aims of this study were to investigate the feedback mechanisms of bank retreat and the lateral erosion characteristics of debris flow surges. Physical experiments were conducted to explore the relationship between the erosion efficiency of debris flows and the geomorphic process of banks, considering the variations in the particle composition of bank soil and multiple debris flow surges. Moreover, a parameterized model for bank retreat was developed.

2. Materials and Methods

2.1. Experimental Setup

The experiments were conducted at the Dongchuan Debris Flow Observation and Research Station, Chinese Academy of Sciences, Yunnan, China. The experimental setup comprised a hopper and a flume, as shown in Figure 1. The hopper served as a temporary storage unit for the debris flow mixture and controlled its release into the flume using two valves to regulate the opening time and size. The flume was constructed with acrylic and had a rectangular cross-section, measuring 5.0 m in length, 0.4 m in width, and 0.4 m in height. The flume was divided

WANG ET AL. 2 of 17



Table 1 *Experimental Arrangement and Test Conditions*

		Bank soils						
Case	D_{50} (mm)	$D_{\rm c}$ (mm)	μ (-)	$\rho_{\rm d}~({\rm kg/m^3})$	ω (-)			
Case 1	7.44	10.47	0.0075	1,682	0.12			
Case 2	4.14	6.73	0.0140	1,661	0.12			
Case 3	3.30	7.19	0.0279	1,736	0.13			
Case 4	2.24	4.99	0.0340	1,693	0.14			
Case 5	0.99	6	0.0537	1,621	0.13			

Note. In each case, there are 10 debris flow surges with $C_{\rm v}=0.50$ and $V_{\rm d}=31.3$ L. ω represents the gravimetric water content.

into three sections: incoming flow section, erosion section, and tailing section (Figure 1a). In the incoming flow section, which spanned 3 m, a non-erodible slope composed of acrylic material was situated on the left bank. This slope had a triangular cross-section with a slope angle (α) of 35° (Figure 1a-1). The purpose of this section was to stabilize the flow pattern of the debris flow, and kinematic parameters of debris flow were measured downstream of this section (Section 1 in Figure 1a) using ultrasonic a distance sensor and a video camera. The erosion section, which was 1 m in length, featured an erodible soil slope on the left bank, mirroring the cross-section of the incoming flow section. The tailing section, also 1 m in length, had the same structure as the incoming flow section. By referring to field cases and previous experimental studies (Hungr, 2005; Rickenmann, 1999), the slope of the flume bed ($S_{\rm bed}$) was set to 20%.

2.2. Experimental Design and Measured Variables

Table 1 presents the experimental arrangement and test conditions. We conducted multiple debris flow surges to erode five different types of bank soils (Case 1–5). Each case consisted of ten debris flow surges with the same material composition and volume, which were labeled as S1-10, respectively. The time interval between adjacent surges in each experimental case was approximately 4 min. During these time intervals, the morphological characteristics of the bank slope were captured using a three-dimensional (3D) laser scanner (Trimble. X7, $6.40 \pm 0.07 \text{ pts./cm}^2$), and the collected point cloud data were utilized to generate digital elevation models (DEMs). The volume and distribution characteristics of bank erosion were then determined by comparing repeat DEMs (Brasington et al., 2012; Yang et al., 2021). The erosion process was recorded by a video camera at the top of the flume (ZED 2 i, 1,920 × 1,080 pixels, 30 fps) (Figure 1a) and by another video camera on the right side of the flume (SONY FDR-AX60, 4,096 × 2,160 pixels, 50 fps). The flow process and depth (h) of the debris flow at cross-section 1 in Figure 1a were documented using an ultrasonic distance sensor (CONTROLWAY mic+, accuracy: 0.1 mm, sampling frequency: 100 Hz). A video camera (GoPro Hero7 Black, 4,096 × 2,160 pixels, 50 fps) atop the flume was employed to measure the surface flow velocity (v) of the debris flow, which was assisted by tracer particles.

2.3. Materials and Applicability

The granular material used for the tests was obtained from the deposition fan of Jiangjia Gully, Yunnan, China, which is known for debris flows. Particles with diameters larger than 20 mm were removed (Chen et al., 2018; Cui et al., 2015; Li et al., 2019). The particle size distributions of the debris flows and the bank soils are illustrated in

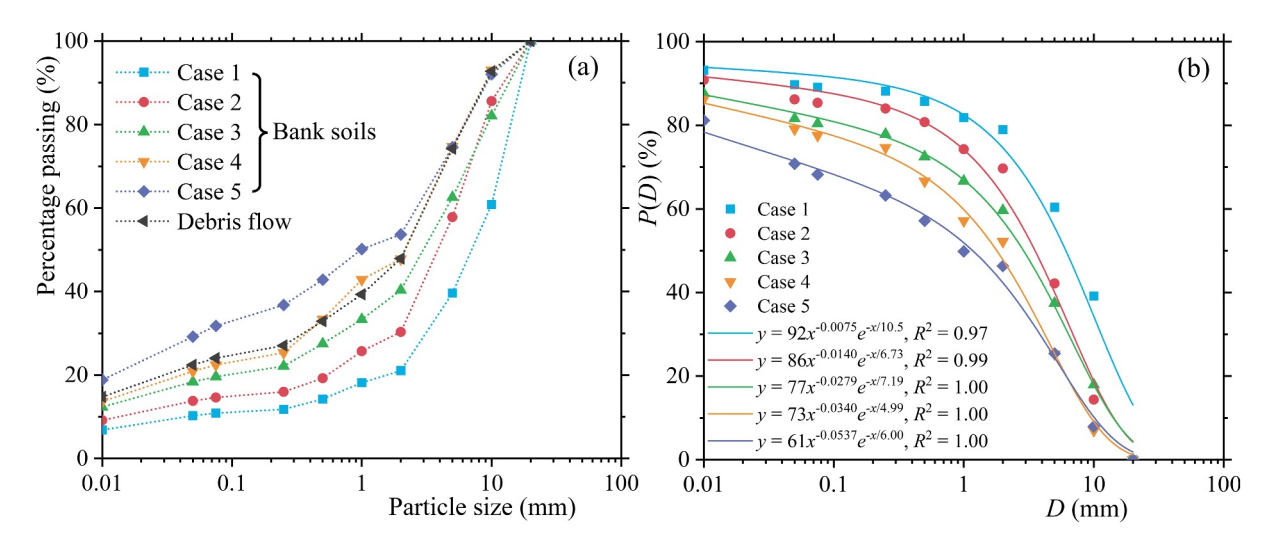


Figure 2. Particle size distributions of channel bank soils and debris flows. (a) Classic cumulative distribution plot. (b) Fitted cumulative distribution curve of Equation 1.

WANG ET AL. 3 of 17

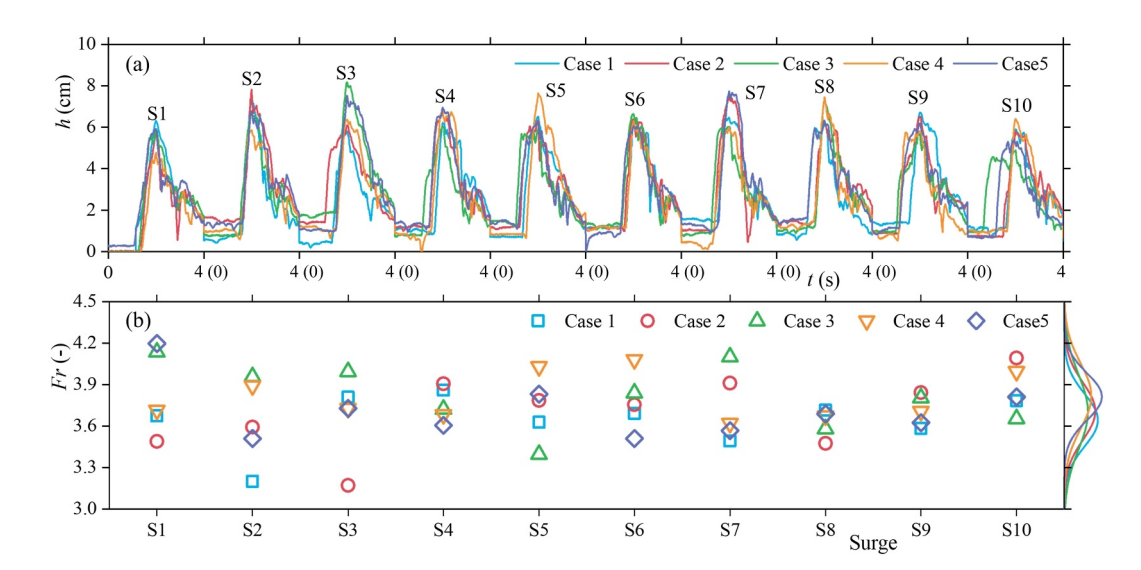


Figure 3. (a) Flow depth and (b) Froude number values of debris flow surges at cross-section 1 in Figure 1a.

Figure 2a and the measured density of the particle material (ρ_s) was 2,680 kg/m³. We utilized the research conducted by Li et al. (2013) to parameterize the particle size distribution characteristics of bank soils:

$$P(D) = CD^{-\mu} \exp(-D/D_c) \tag{1}$$

where D is the particle size (mm); P(D) is the mass percentage of particles > D; D_c is a characteristic size and roughly features the particle size range (mm); μ is a power exponent describing the fine particle content of soils; and the coefficient C is related to μ (Li et al., 2017). The parameter pair (μ , D_c) notably influences the erosion of debris flow dams (Ruan et al., 2021). Utilizing the aforementioned method, we analyzed of the particle size distribution of the bank soil (refer to Figure 2a). The figure clearly showed that Equation 1 adeptly captured the particle size distribution of bank soil ($R^2 \ge 0.97$). Notably, within this investigation, disparities in the particle size distribution of bank soil were primarily apparent in the parameter μ (Figure 2b and Table 1), because of our control over the particle size range.

Achieving precise scaling in debris flow experiments poses significant challenges (Iverson, 2015). In our experiments, we did not use specific field cases as prototypes. Instead, we aimed for a rough similarity in the compositions and movements of debris flows by controlling dimensionless parameters. The debris flows exhibited a sediment volume fraction (C_v) of 0.5 in this study; this value was considered reasonable based on findings from field investigations (Church & Jakob, 2020; Iverson, 1997). Each debris flow surge had a volume (V_d) of 31.3 L, comprising 42.0 kg of sediment and 15.7 kg of water. Considering the characteristic open-channel gravity flow behavior of debris flows, we regulated the Froude number (Fr) during the experiments. While the calculation formula for the Fr of debris flow is recommended in various studies (Choi et al., 2015; Domnik & Pudasaini, 2012; Pudasaini & Domnik, 2009), this study necessitated consideration of the influence of trapezoidal open-channel cross-sections on the Froude number (French, 1985):

$$Fr = \frac{v}{\sqrt{g\cos\theta(A/B)}}\tag{2}$$

where v is the average velocity of cross-section 1 in Figure 1a (m/s), which was substituted with the approximate surface flow velocity measured in this study; g is the gravitational acceleration, $g = 9.8 \text{ m/s}^2$; θ is the bed slope angle of the flume, $\theta \approx 11.3^\circ$; A is the cross-sectional area of flow (m²), $A = hb_0 + 0.5 h^2/\tan\alpha$; B is the flow width at the free surface (m), $B = b_0 + h/\tan\alpha$; h is the flow depth of debris flow at cross-section 1 in Figure 1a; b_0 is the initial width of the channel bed, $b_0 = 0.1 \text{ m}$; and α is the initial slope of the channel bank, which is approximately 35° in this study.

WANG ET AL. 4 of 17



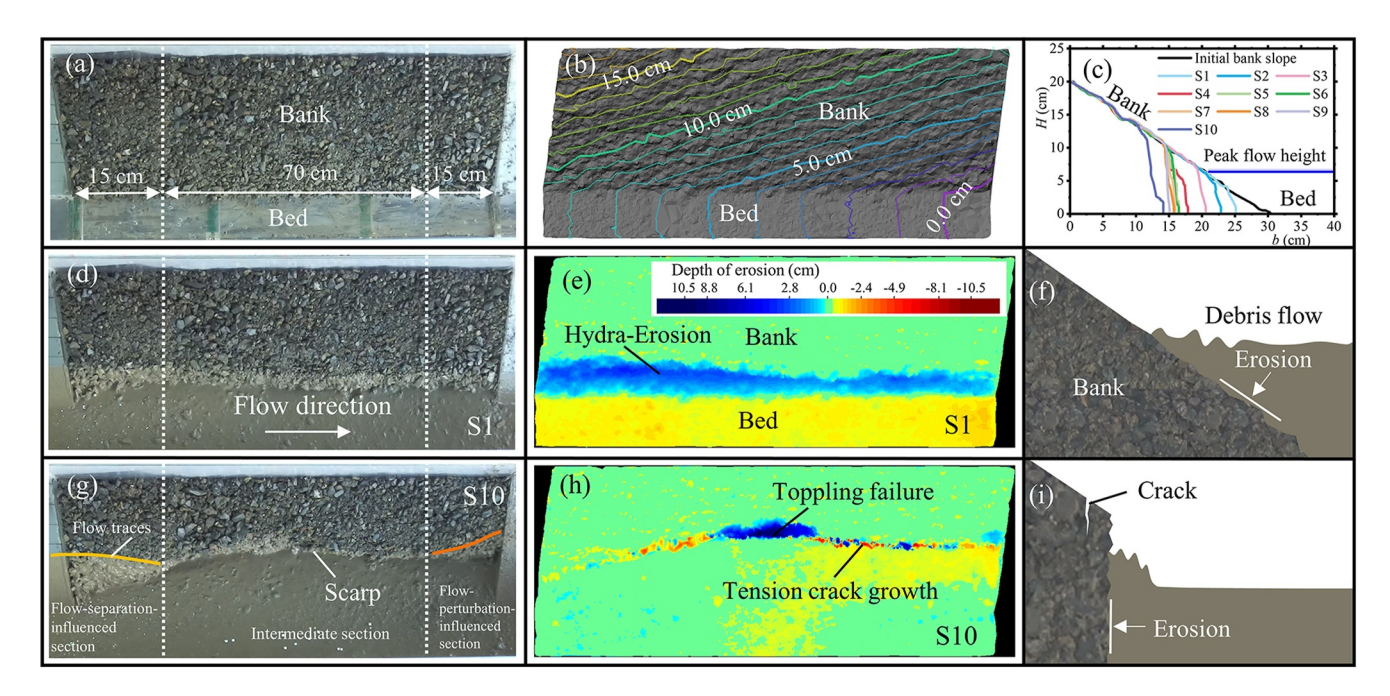


Figure 4. Bank retreat processes (Case 1). (a) and (b) Top view and contour map of the initial erodible bank; (c) bank retreat process at cross-section 2 in Figure 1a; (d) and (g) top views after 1 and 10 debris flow surges; (e) and (h) erosion distributions of the S1 and S10 debris flow surges; and (f) and (i) erosion mechanisms of the S1 and S10 surges (Schematic diagram).

The h of each surge process has peak values ranging from 4.8 to 8.2 cm (Figure 3a). The mean and standard deviation of peak h for each surge were 6.4 and 0.7 cm, respectively. The Fr corresponding to peak h ranged from 3.2 to 4.2 (Figure 3b), which was considered reasonable based on Fr from field cases (Du et al., 2023; Guo et al., 2020; Wang et al., 2022; Zhou et al., 2019). Moreover, the erodible banks were prepared through the following steps: bank soils were paved in a layer-by-layer manner (not compacted), and each layer was approximately 20 mm in thickness. An electric spray system was employed to apply a controlled quantity of water for each soil layer, regulating the gravimetric water content (ω). The dry densities (ρ_d) of the bank soils were computed based on the mass of utilized soil particles and the volume of the erodible gully banks, which varied between 1,621 and 1,736 kg/m³ (Table 1). The ω value of the bank soil were assessed before and after the erosion tests, by utilizing a handheld soil volumetric water content measuring instrument (METER TEROS 10) and the drying method, respectively. The ω values were determined to range from 0.12 to 0.14 (Table 1).

3. Results and Analysis

3.1. Bank Retreat Process

Figure 4 illustrates the bank retreat process using Case 1 as an example. Figures 4a and 4b display the initial characteristics of the erodible bank, while Figure 4c demonstrates the bank retreat process at cross-section 2 in Figure 1a. Figures 4d–4f depict the erosion distribution and mechanism of the first debris flow surge (S1), while Figures 4g–4i show the erosion distribution and mechanism of the last debris flow surge (S10). Based on the differences in erosion mechanisms, the bank retreat process was divided into two stages:

Toe Cutting Stage (Figures 4d, 4e, and 4f): During the initial erosion stage, hydraulic erosion dominated. The slope of the bank toe was small and the debris flow covered the bank toe (Figure 4f). The contact area between the debris flow and the bank soil was large, and the erosion process was controlled by the shear stress between them. As the shear force and erosion rate of the debris flow are positively correlated with the flow depth (Pudasaini & Fischer, 2020), the slope of the bank toe gradually increased and eventually formed a scarp (Figure 4c). With the widening of the channel bed, the scarp height increased and the bank stability decreased.

Bank Collapse Stage: During this phase, the retreat of the bank resulted from the combined effects of hydraulic erosion and gravity erosion. A steep scarp, with a slope approaching 90°, formed at the bank toe (refer to

WANG ET AL. 5 of 17

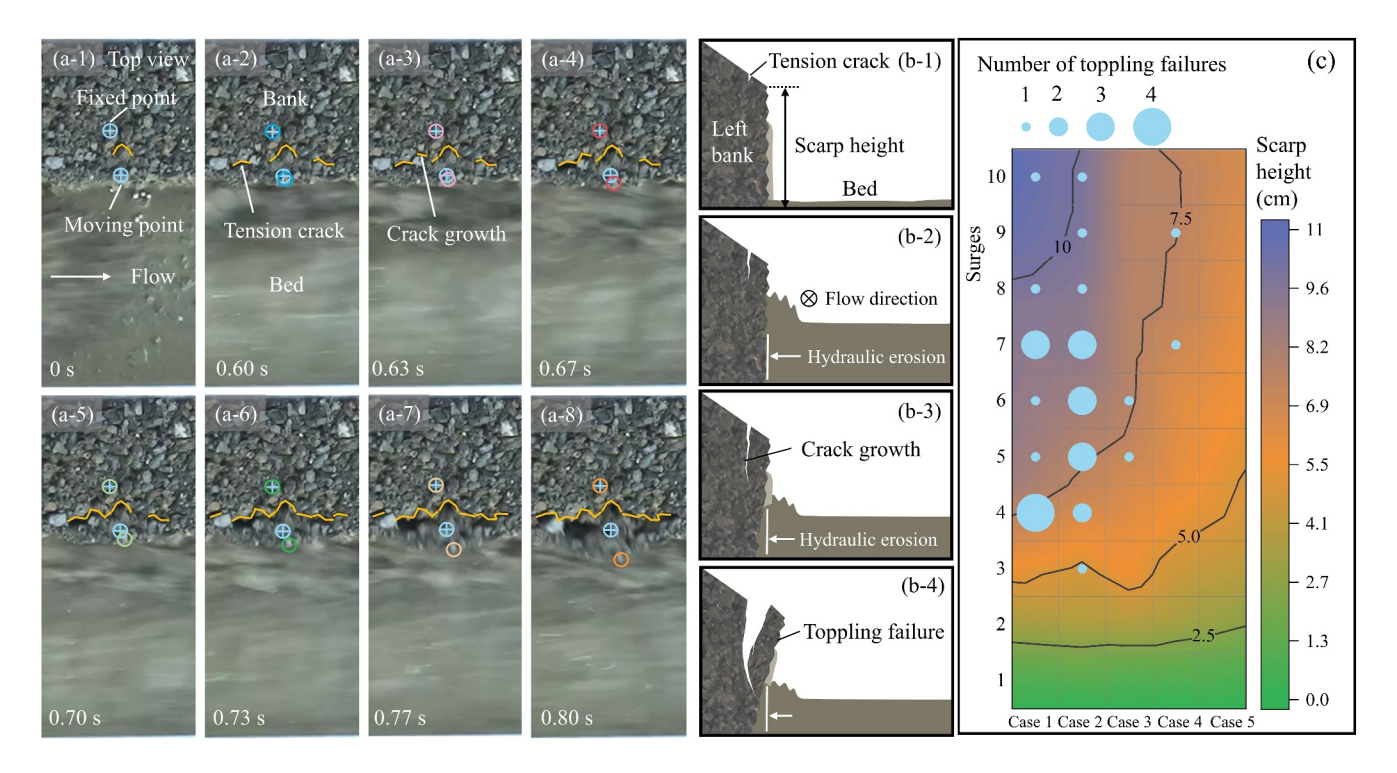


Figure 5. Toppling failure processes (S10, Case 1). (a) Top view of the toppling failure process; (b) schematic diagram of the toppling failure process; and (c) distribution of the number of toppling failures in different cases and surges.

Figures 4g-4i), and the hydraulic erosion direction of the debris flow was nearly horizontal, pointing toward the interior of the bank. Because flow depth controls hydraulic erosion (Iverson, 2012; Pudasaini & Fischer, 2020), the soil at the base of the scarp experienced the most significant hydraulic erosion. Moreover, the undermining of the debris flow at the bank toe led to gravity failure in the form of toppling failure (see Figure 5). Figures 5a and 5b illustrate the development of tension cracks and the process of toppling failure under the influence of the debris flow. Figure 5c provides a distribution map of the number of toppling failures. Toppling failures were observed after the scarp height reached a critical threshold. The frequency of such failures exhibited a gradual decline with an increase in the fine particle content of the bank soil. This trend was partially attributed to the influence of cohesion on the width of failure blocks (Osman & Thorne, 1988; Thorne, 1978). However, the number of failures within a debris flow surge progressively diminished at the final stage (refer to Figure 5c). This decline was attributed to the substantial widening of the channel bed, the reduction in debris flow depth, and the diminished disturbance caused by the debris flow at the bank toe.

As depicted in Figure 4g, noticeable differences from the middle section were observed in the erosion topography near the upstream and downstream fixed banks. This discrepancy was attributed to flow separation and disturbances arising from the discontinuity between the erodible and fixed banks. To minimize the influences of fixed banks on the erosion data, test data within a 15 cm range near the fixed banks were excluded.

Furthermore, we noted bank erosion associated with fluctuations in debris flow depth. As the debris flow head traversed a cross-section, there was a rapid reduction in the flow depth (see Figure 6a) in that specific region. Concurrently, a considerable volume of debris flow slurry adhered to the bank soil, displaying a downwards creeping behavior. This slurry aided the displacement of certain soil particles or clusters (Figure 6). This process recurred multiple times with successive debris flow surges. However, this form of erosion did not predominate.

The progression characteristics of the cumulative bank erosion volume ($V_{\rm ero}$) under various bank soil conditions are shown in Figure 7. In all scenarios, with the accumulation of debris flow surges, $V_{\rm ero}$ steadily increased. However, the rate of increase gradually decreased. This phenomenon was ascribed to a negative feedback mechanism, where the geomorphic alterations stemming from bank retreat weakened the primary factor (flow depth) controlling and inducing bank erosion. Furthermore, an increase in the coarse particle content of the bank

WANG ET AL. 6 of 17

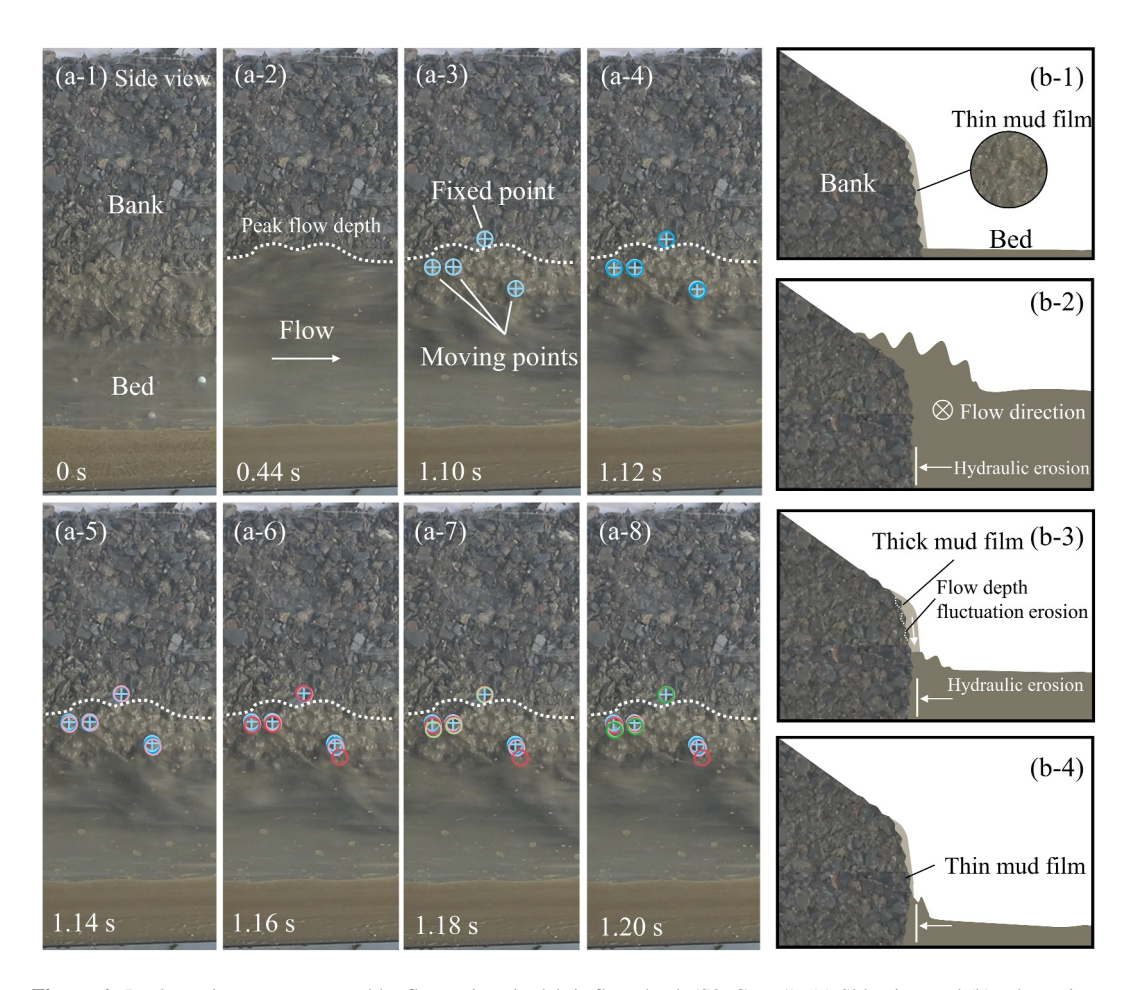


Figure 6. Bank erosion process caused by fluctuations in debris flow depth (S3, Case 1). (a) Side view and (b) schematic diagram.

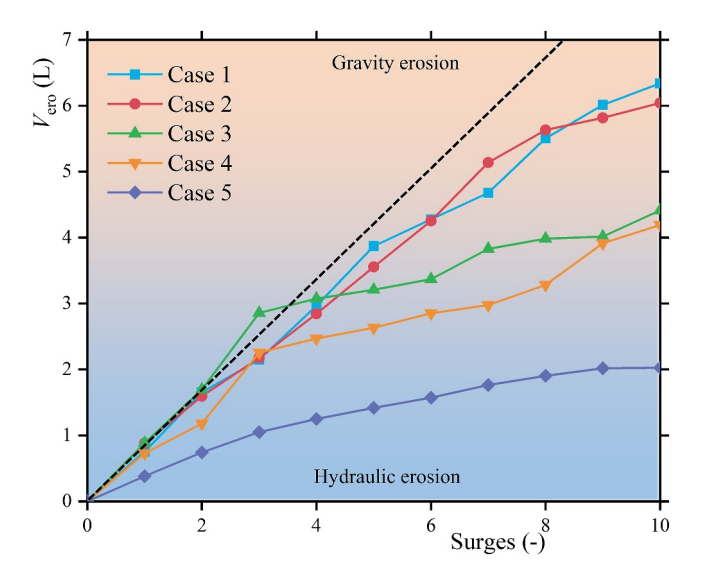


Figure 7. Progression of cumulative bank erosion volume. The diagonal line illustrates the developmental trend of $V_{\rm ero}$ when the erosion efficiency of the debris flow remained constant. As $V_{\rm ero}$ increases, the scarp height gradually increases (Figures 4 and 5), and the primary erosion mechanism shifts from hydraulic erosion to gravity erosion.

soils gradually increased the debris flow erosion volume. This increase was attributed to heightened hydraulic erosion and toppling failures resulting from a reduction in soil cohesion and tensile strength.

3.2. Bed Widening and the Erosion Efficiency of Debris Flow

The widening of the channel bed resulting from bank retreat reduced the flow depth of the debris flow, which contributed to the gradual decrease in the increase rate of the $V_{\rm ero}$ value, as shown in Figure 7. To further explore the relationship between bed widening and the erosion efficiency of debris flows, the bed widening was quantified by the relative bed widening width:

$$b_e^* = \frac{b_e}{b_0} = \frac{b - b_0}{b_0} \tag{3}$$

where b and b_0 denote the width and initial width of the channel bed, respectively; $b_{\rm e}$ represents the bed widening width; $b_{\rm e}$ * represents the relative bed widening width.

According to previous research (Sawaske & Freyberg, 2012; Wang et al., 2022), the erosion efficiency with respect to erosion length was defined as follows:

WANG ET AL. 7 of 17



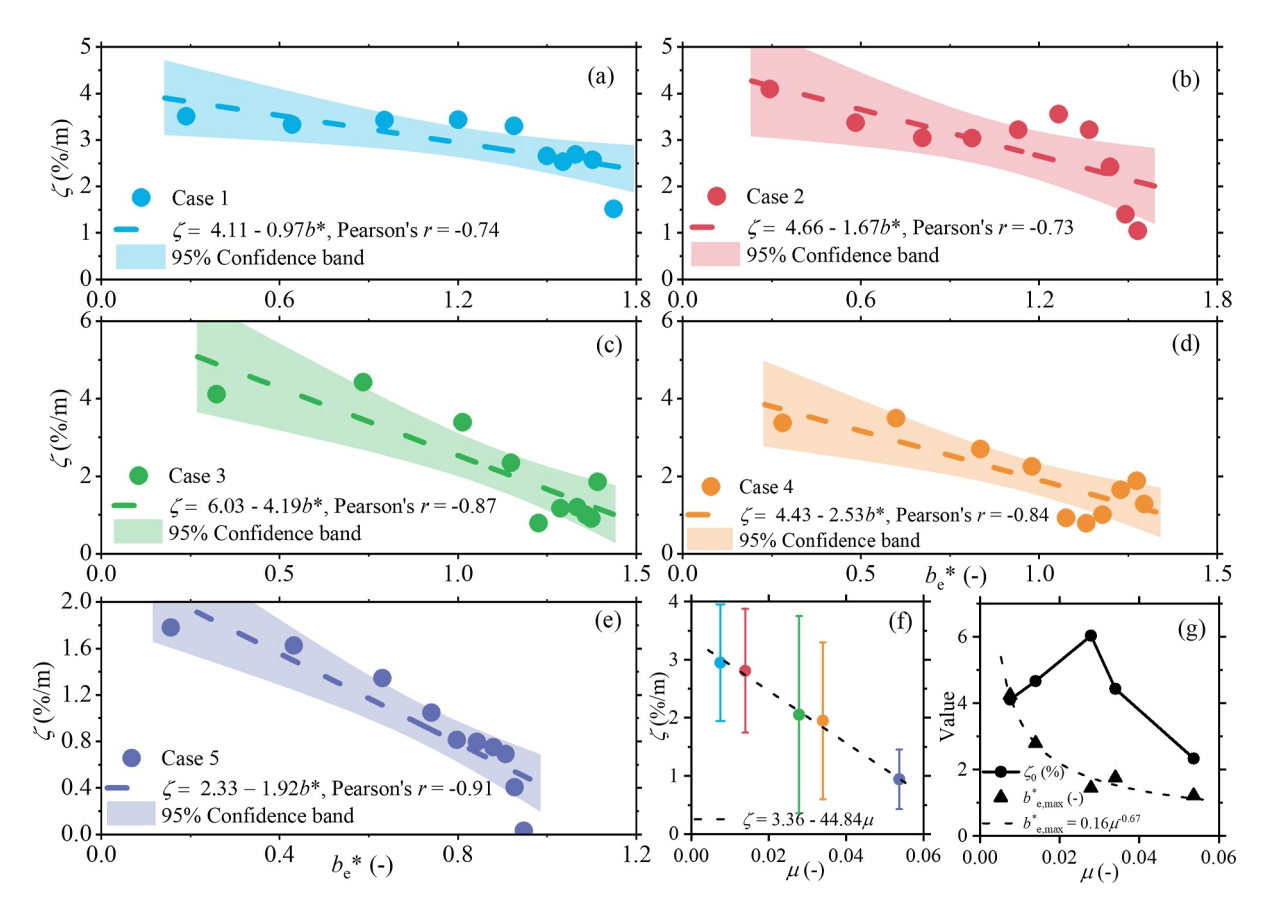


Figure 8. The relationship between ζ and b_e^* : (a) Case 1; (b) Case 2; (c) Case 3; (d) Case 4; (e) Case 5. (f) Relationship between ζ and μ ; the error bars represent the differences in ζ between debris flow surges. (g) Impacts of μ on ζ_0 and $b_{e,\max}^*$.

$$\zeta = \frac{\Delta V_{ero} / L_{pote}}{\Delta V_D} \tag{4}$$

where $\Delta V_{\rm ero}$ and $\Delta V_{\rm D}$ indicate the variation of cumulative bank erosion volume and cumulative debris flow volume, respectively; ζ represents the erosion efficiency with respect to erosion length and it is dimensional; $L_{\rm pote}$ represents the length of the potential bank erosion section, the focus of this study is the 0.7 m of the intermediate section in Figure 4g, $L_{\rm pote}=0.7$ m.

In this study, all debris flow surges have same volume ($\Delta V_{\mathrm{D,i}} = V_{\mathrm{d}} = 31.3~\mathrm{L}$). ζ_{i} represents the erosion efficiency with respect to erosion length of the *i*th debris flow surge. When $i=2,\ldots,9$, we replaced ζ_{i} with the average values of $\zeta_{\mathrm{i-1}}$, ζ_{i} and $\zeta_{\mathrm{i+1}}$ (average erosion efficiency of three adjacent debris flow surges) to weaken the impact of the randomness of toppling failures on the experimental data. Correspondingly, we replaced $b_{\mathrm{e,i}}$ * with the average values of $b_{\mathrm{e,i-1}}$ *, $b_{\mathrm{e,i}}$ * and $b_{\mathrm{e,i+1}}$ *. Specifically, the $b_{\mathrm{e,i}}$ * and ζ_{i} were calculated using the following equation. The calculation results are shown in Figure 8.

$$b_{e,i}^* = \begin{cases} \frac{b_{e,i} + b_{e,i-1}}{2b_0}, i = 1,10\\ \frac{b_{e,i+1} + 2b_{e,i} + 2b_{e,i-1} + b_{e,i-2}}{6b_0}, i = 2,...,9 \end{cases}$$
(5)

WANG ET AL. 8 of 17



Table 2Particle Size Distribution Parameters of Bank Soil and the ζ Attenuation Model Parameters

	Bank soils			Parameters of ζ attenuation model		
Case	D_{50} (mm)	$D_{\rm c}$ (mm)	μ (–)	ζ_0 (%/m)	k (-)	$b_{e,\max}^*$ (-)
Case 1	7.44	10.47	0.0075	4.11	0.97	4.24
Case 2	4.14	6.73	0.0140	4.66	1.67	2.79
Case 3	3.30	7.19	0.0279	6.03	4.19	1.43
Case 4	2.24	4.99	0.0340	4.43	2.53	1.75
Case 5	0.99	6	0.0537	2.33	1.92	1.21

$$\zeta_{i} = \begin{cases}
\frac{\Delta V_{ero,i} / L_{pote}}{\Delta V_{D,i}}, i = 1,10 \\
\frac{\sum_{i=1}^{i+1} \Delta V_{ero,i} / L_{pote}}{\sum_{i=1}^{i+1} \Delta V_{D,i}}, i = 2,...,9
\end{cases}$$
(6)

where $b_{\rm i}$ and $b_{\rm e,i}$ (i=1,2,3,...,10) represent the bed width and the bed widening width of after the *i*th debris flow surge, respectively; $b_{\rm e,i}$ * represent the relative bed widening width when the *i*th debris flow surge pass through erodible bank. $\Delta V_{\rm ero,i}$ and $\Delta V_{\rm D,i}$ (i=1,2,3,...,10) indicate bank erosion volume and debris flow volume of the *i*th debris flow surge, respectively. Specifically, bed width was measured at cross-section 2 (Figures 1a and 4c).

By utilizing the experimental data illustrated in Figures 8a–8e, apronounced by was identified. In all cases, the absolute values of Pearson's reverseded 0.7

negative correlation between ζ and b_e^* was identified. In all cases, the absolute values of Pearson's r exceeded 0.7 (Figures 8a–8e), indicating a strong linear correlation. To quantify this relationship, a linear function model was selected:

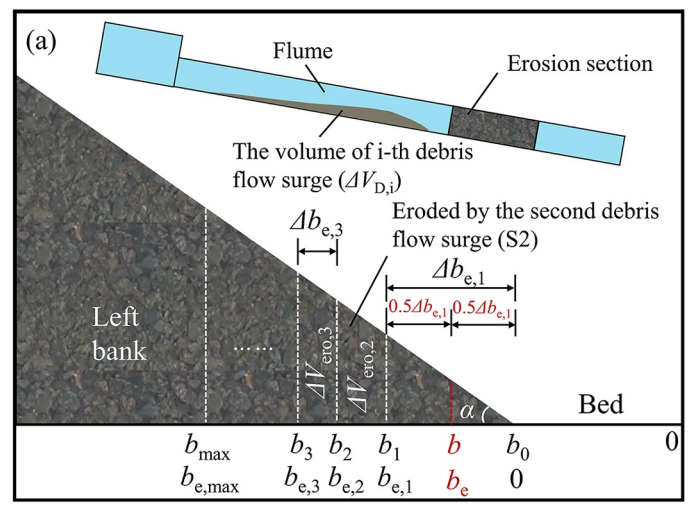
$$\zeta = \zeta_0 - k \cdot b_a^* \tag{7}$$

where ζ_0 denotes the initial erosion efficiency with respect to erosion length; k represents the attenuation coefficient of erosion efficiency that signifies the influence of bed widening and flow depth decline on erosion; and $b_{e,\max}^* = \zeta_0/k$ represents the maximum relative bed widening width. The ζ_0 initially increased and subsequently decreased with the increase of μ (representing the fine particle content), peaking at 6.03%/m when $\mu = 0.028$ (Table 2 and Figure 8g). Moreover, $b_{e,\max}^*$ decreased as μ increased, and these two variables displayed a strong power function relationship ($R^2 = 0.97$) (Figure 8g). Furthermore, the mean value of ζ exhibited a linear negative correlation with μ , as depicted in Figure 8f. The error bars in the figure denote the variations in ζ among different surges. This phenomenon highlighted the substantial influences of the particle composition of bank soil on the entire process of bank retreat.

4. Discussion

4.1. A Parameterized Model Describing the Bank Retreat Process in a Debris Flow Channel

Based on the experimental observations (see Figure 4c), we present a conceptual model of bank retreat (see Figure 9a). It is crucial to acknowledge that this conceptual model is specifically relevant to banks characterized



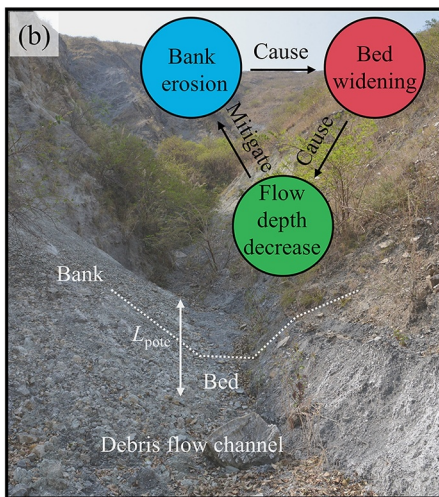


Figure 9. (a) Sketch of the bank retreat process with multiple debris flow surges. (b) Mechanism of the debris flow channel bank retreat.

WANG ET AL. 9 of 17



by modest heights and broadly graded soils. In contrast, for high banks and non-cohesive soils, shear failure tends to be the dominant mode of bank failure, unlike the toppling failure emphasized in this study (Lyu et al., 2017; Thorne & Tovey, 1981; Zhao et al., 2019).

According to Figure 9a, the relationship between $\Delta V_{\rm ero}$ and $\Delta b_{\rm e}$ was obtained:

$$\Delta V_{ero} = \frac{1}{2} \left(\left(b_e + \frac{1}{2} \Delta b_e \right) + \left(b_e - \frac{1}{2} \Delta b_e \right) \right) \tan \alpha \cdot \Delta b_e \cdot L_{pote} = b_e \tan \alpha \cdot \Delta b_e \cdot L_{pote}$$
 (8)

where $\Delta b_{\rm e}$ is the variation in $b_{\rm e}$ ($\Delta b_{\rm e} = b_{\rm e} - b_{\rm e-1}$), and α represents the initial slope of the channel bank, which is approximately 35° in this study.

Combining Equations 3, 4 and 8 yields the following expression:

$$\zeta = \frac{b_0^2 b_e^* \tan \alpha \Delta b_e^*}{\Delta V_D} \tag{9}$$

where Δb_e^* represents the relative variation in b_e ($\Delta b_e^* = \Delta b_e/b_0$).

Substituting $M = \tan \alpha / b_0$, a parameter characterizing the geomorphological characteristics of the erosion section channel, into Equation 9 yields the following:

$$\zeta = \frac{Mb_e^* \Delta b_e^*}{\Delta V_D^*} \tag{10}$$

where $\Delta V_{\rm D}^*$ represents the relative variation of cumulative debris flow volume ($\Delta V_{\rm D}^* = \Delta V_{\rm D}/b_0^3$) and b_0^3 is a volume scale (Wang et al., 2022).

We discerned a clear pattern in the intricate interplay of hydraulic erosion and toppling failure: ζ exhibits a strong linear negative correlation with b_e^* (Figures 8a–8e). This correlation can be attributed to a negative feedback loop in which bank erosion leads to channel bed widening, thereby reducing flow depth and subsequently mitigating bank erosion (Figure 9b). Previous experiments have shown a gradual decrease in debris flow density with the widening of the channel bed, indirectly supporting the negative feedback relationship between debris flow erosion efficiency and bed widening (Zhou et al., 2015). Furthermore, the linear relationship between ζ and b_e^* facilitates the establishment of a function linking b_e^* to the activities of multiple debris flow surges characterized by the relative accumulated volume of the debris flow (V_D^*). Combining Equations 7 and 10 yields the following equation:

$$\frac{\Delta b_e^*}{\Delta V_D^*} = \frac{\zeta_0}{M b_e^*} - \frac{k}{M} \tag{11}$$

Assuming that $b_e^* = f(V_D^*)$ is continuous and differentiable, Equation 11 can be transformed into the following expression:

$$\frac{\partial b_e^*}{\partial V_D^*} = \frac{\zeta_0}{M b_e^*} - \frac{k}{M} \tag{12}$$

Solving Equation 12 yields the following equation:

$$\frac{-Mb_e^*}{k} - \frac{M\zeta_0}{k^2} \ln \left(\frac{\zeta_0 - kb_e^*}{M} \right) = V_D^* + C$$
 (13)

According to the initial condition (when $V_D^* = 0$, $b_e^* = 0$), C can be calculated as $C = -\frac{M\zeta_0}{k^2} \ln\left(\frac{\zeta_0}{M}\right)$. Substituting C and $k = \zeta_0/b_{e,\max}^*$ into Equation 13 yields the following:

WANG ET AL. 10 of 17

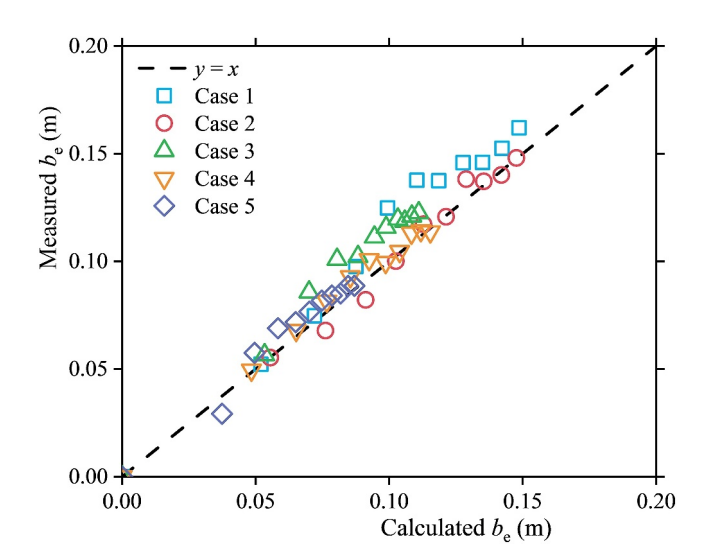


Figure 10. Comparison of computed and measured bank retreat distances.

$$\ln\left(1 - \frac{b_e^*}{b_{e,\text{max}}^*}\right) + \frac{b_e^*}{b_{e,\text{max}}^*} = -\frac{\zeta_0}{M(b_{e,\text{max}}^*)^2} V_D^*$$
 (14)

Equation 14 is a calculation model for the relative bed widening width that comprehensively considers the initial erosion efficiency with respect to the erosion length (ζ_0) , the maximum relative bed widening width $(b_{e,\max}^*)$, the channel topography (M) and the debris flow activity (V_D^*) . Notably, Equation 14 applies exclusively to erodible channel banks. In cases where a bank is non-erodible $(b_{e,\max}^* > 0)$, a scenario where $b_e^* = 0$ signifies no debris flow eroded banks $(V_D^* = 0)$, and both sides of Equation 14 are equal to 0. Conversely, when $b_e^* = b_{e,\max}^*$, indicating the termination of bank erosion by the debris flow, the left side of Equation 14 approaches - ∞ . If Equation 14 holds under such circumstances, V_D^* becomes ∞ , suggesting that achieving $b_e^* = b_{e,\max}^*$ is unattainable under limited debris flow volume. This phenomenon may arise from the fact that as b_e^* approaches $b_{e,\max}^*$, ζ approaches zero (see Equation 7), rendering the incremental debris flow (ΔV_D) with limited volume

insufficient to induce erosion. Moreover, we substituted the experimentally derived empirical values of ζ_0 and $b_{e,\max}^*$ (Table 2) into Equation 14. Subsequently, we calculated the evolution process of b_e^* under various working conditions (Cases 1–5) using the process of cumulative debris flow volume (V_D) employed in the experiment. Finally, we determined the evolution process of bank retreat distance (b_e) based on Equation 6 (Figure 10). The figure illustrates a close alignment between the calculated and measured values of b_e , affirming that Equation 14 holds the potential to accurately simulate the process of debris flow bank retreat.

Equation 14 offers a straightforward method for assessing bank retreat processes in debris flow channels. For instance, in cases where only limited data for $b_{\rm e}^*$ and $V_{\rm D}^*$ are available, this approach can be instrumental for evaluating and predicting the overall bank retreat process (achieved by inversely determining ζ_0 and $b_{e,{\rm max}}^*$ based on limited data). Moreover, when assessing ζ_0 and $b_{e,{\rm max}}^*$ through theoretical analysis, the physical process of bank retreat in debris flow gullies should be seriously considered. We categorized bank retreat process into two stages (Section 3.2): toe cutting, primarily influenced by hydraulic erosion, and bank collapse, governed by a combination of hydraulic and gravity erosion. Specifically, there are two considerations to note. First, the current debris flow hydraulic erosion models (Haas and Woerkom, 2016; Iverson, 2012; Pudasaini & Krautblatter, 2021; Takahashi, 2007) are primarily designed for bed erosion (with the erosion direction being vertically downwards). The suitability of these models for hydraulic erosion of banks (where the erosion direction is inclined or horizontal, as shown in Figures 4f and 4i) merits further investigation in future research. Second, the factor of bank collapse requires comprehensive consideration. Previous investigations have demonstrated the prevalence of bank collapse in an analogous process, the riverbank retreat process (Gong et al., 2018; Zhao et al., 2020). Solely considering hydraulic erosion of debris flow leads to underestimated values of bank erosion volume than actual observations (Mergili et al., 2020).

4.2. Influences of μ on ζ_0 and $b_{e,\text{max}}^*$

The primary parameters of the bank retreat model (Equation 14) are ζ_0 and $b_{e,\text{max}}^*$. Utilizing experimental data, we established an empirical relationship (Figure 8g) between these parameters and a scaling distribution parameter (μ) characterizing the fine particle content of the bank soils (Li et al., 2013).

The ζ_0 exhibited an increase followed by a decrease with the increase of μ , reaching its maximum value of 6.03%/m when $\mu = 0.028$ (Figure 8g). This result can be attributed to the following considerations. When the fine particle content of the bank soil is low ($\mu < 0.028$ in this study), the bank soil exhibits characteristics closer to those of non-cohesive soil, and the critical shear stress is primarily influenced by the coarse particle size (Shields' Entrainment Criterion) (Brunier-Coulin et al., 2020; Davidson & Eaton, 2018). Conversely, when the fine particle content of the bank soil is high ($\mu > 0.028$ in this study), the cohesion of the bank soil gradually increases (Kim et al., 2005; Kouakou et al., 2020), thereby exerting a dominant influence on the increase in critical shear stress

WANG ET AL. 11 of 17



(Darby et al., 2010; Wu et al., 2018; Yao et al., 2022) as μ increases. Analogous phenomena have been observed in physical model experiments focusing on bed erosion (Yao et al., 2022).

The parameter $b_{e,\max}^*$ decreases with increasing μ , revealing a strong power function relationship as depicted in Figure 8g. The relationship between $b_{e,\max}^*$ and μ is different from that between ζ_0 and μ , which may be caused by that $b_{e,\max}^*$ is affected by gravity erosion in addition to hydraulic erosion (Figure 5). As the fine particle content (μ) decreases, the cohesion of the bank soil gradually decreases (Kim et al., 2005; Kouakou et al., 2020). Consequently, this decrease in cohesion contributes to the progression of tensile cracks and toppling failure (Figure 5c and Alzo'ubi et al., 2010; Zhang et al., 2021; Zhao et al., 2022). Additionally, cohesion significantly impacts the bank retreat process in rivers by affecting the width of failure blocks (Osman & Thorne, 1988; Thorne, 1978).

In the soil particle size distribution model (Equation 1) proposed by Li et al. (2013), there is an important parameter D_c , which, apart from μ , is a characteristic size roughly representing the particle size range (Li et al., 2017). The above discussion regarding the role of μ is conducted under conditions where D_c is relatively stable (with the experimental control ensuring that the particle size of the channel bank soil is less than 20 mm). It is imperative to carefully consider the scale effects: when the value of D_c significantly exceeds the range of our experiment, a thorough reexamination of the aforementioned discussion, especially the numerical results, is warranted.

4.3. 'Basal Endpoint Control' in the Bank Retreat Process of Debris Flow Channel

The concept of 'Basal Endpoint Control' was originally proposed by Carson and Kirkby (1972) for hill slopes and later modified by Thorne (1978, 1982) to apply to retreating stream banks. Based on the 'Basal Endpoint Control' concept, the bank slopes can be divided into three states: (a) Impeded Removal, where the sediment supply rate from geotechnical failures and upstream channel to the toe exceeds the ability of the local flow to remove sediment, resulting in bank toe advance and a gradual reduction in slope angle. (b) Unimpeded Removal, where sediment supply and removal are balanced, keeping the bank toe stable; and (c) Excess Basal Removal, where the capacity for sediment removal surpasses sediment supply, leading to bank toe retreat and a steeper bank angle. The retreat process of debris flow channel banks also follows the 'Basal Endpoint Control' principle. During inter-event periods of debris flow activity, the banks are in the first or second state, with sediment removal capacity being weak. The accumulation of sediment at the toe due to impeded removal leads to bank toe advance and the formation of small slope angles, as shown in the background photo of Figure 9b. When debris flows occur, the sediment transport capacity increases sharply, and the banks enter the third state, with rapid removal of sediment at the toe and a sharp increase in slope angle, as observed in Figure 4. With the cessation of debris flow activity and the onset of an inter-event period, a new geomorphological cycle begins.

During the period of debris flow activity, the focus period in this study, the banks are in the third state and evolve toward the second state under the influence of a negative feedback loop (Figure 9b). In the condition of a stable scale of debris flow surges (as controlled in the experiments), the decrease in flow depth due to channel bed widening is considered to greatly contribute the negative feedback loop. During this period, the debris flow's ability to remove sediment from the toe exceeds the supply of sediment from bank failures. The rapid removal of supplied sediment was observed in the experiments (video data in Wang et al., 2024, such as Case 1-S4 and Case 1-S10), which is attributed to the strong sediment transport capacity of debris flows (Cui et al., 2013; Garcia-Martinez & Lopez, 2005) and the steep channel bed. Consequently, the rate of bank retreat is primarily controlled by the erosion rate of in-situ soil at the toe by debris flows. Flow depth, which is closely related to debris flow basal shear stress and erosion (Iverson, 2012; Pudasaini & Fischer, 2020), also becomes the key factor controlling bank retreat. In rivers, there is also a negative feedback relationship between channel widening and bank retreat (Cluer & Thorne, 2014; Zhao et al., 2022), but changes in flow depth do not have a particularly prominent influence in this process. Instead, the near-bank flow velocity is regarded as the key factor affecting bank retreat. This is because bank retreat is controlled by the coarse particle size at the bank toe (Davidson & Eaton, 2018; MacKenzie & Eaton, 2017), and the removal of coarse particles is believed to be primarily governed by the drag and lift forces of the flow (both significantly influenced by flow velocity) (Thorne, 1978). In rivers, the cohesion of bank soil is also considered an important factor, as it significantly affects the state of the supply soil reaching the toe, with a cohesive block of material being more difficult to move than disaggregated particles (Thorne & Tovey, 1981). Moreover, the impact of channel curvature on debris flow bank retreat is not considered in this

WANG ET AL. 12 of 17



study. Curved channels could complicate the issue, such as the effect of secondary flows (Bathurst et al., 1979; Chen & Tang, 2012). Unfortunately, current understanding of secondary flows in debris flows is still limited.

Given that knowledge of riverbank retreat far exceeds that of debris flow channel bank retreat, it is a good option to draw on the researches from riverbank retreat in future studies, while also paying attention to the distinctions in bank retreat between debris flows and rivers. These distinctions may arise from differences in bank material composition (Darby et al., 2010; Parker et al., 2011; Thorne & Tovey, 1981), bank topography (Cui et al., 2013; Lyu et al., 2022; Stecca et al., 2017; Zhao et al., 2022; Zhou et al., 2015), and the physical and mechanical characteristics of debris flows and river flows. Compared to river flows, debris flows contain a higher volume of solid materials such as sediment and driftwood (Chen et al., 2011; Huebl & Kaitna, 2021; Imaizumi et al., 2019) and surge down steeper channels (Kean et al., 2013; Zanuttigh & Lamberti, 2007). These characteristics significantly impact the interaction between the flow and the channel. For example, the regime theory commonly used to evaluate river width (Dunne & Jerolmack, 2020; Yu & Wolman, 1987) may not be directly applicable to debris flow channels. This theory aims to describe the equilibrium state of riverbanks under given discharge (bankfull discharge, Wolman & Miller, 1960) and bank material characteristics. However, debris flow events typically last too briefly to shape and maintain banks in an equilibrium state; additionally, during the intervals between debris flow events, bank advance often occurs due to the supply of material from slopes (Berger et al., 2011; Imaizumi et al., 2019; Schwab et al., 2008). The alternating retreat and advance of the banks are a notable characteristic of debris flow channels. Accordingly, a model that characterizes the bank retreat process rather than the equilibrium state may be more useful, as it better reflects the supply of channel bank material to debris flows and its impact on the magnitude of debris flow hazards.

4.4. Limitations

Due to the influence of scaling effects, the applicability of the bank retreat parameterization model proposed in this study under field conditions still requires further investigation. Before this model can be practically applied, it is essential to conduct verification and calibration studies based on field observation data. In field scenarios, the scale of debris flow surges is not always stable (Lapillonne et al., 2023; Nagl et al., 2024), and the texture of bank soil is not always homogeneous. The retreat process of actual debris flow channel banks may be governed by different equations at different times, with ζ_0 and $b_{e,\max}^*$ in Equation 14 possibly being functions of time. The influencing factors may include debris flow discharge (Lyu et al., 2017), debris flow density, channel bed slope (Zhang et al., 2023), flow depth, bank height (Zhao et al., 2020), bank soil composition and cohesion (Thorne & Tovey, 1981), and bank vegetation (van Dijk et al., 2013; Zhao et al., 2022). Conducting independent field observations and physical experiments to investigate their impact on ζ_0 and $b_{e,\max}^*$ is significant. Moreover, caution is advised when extrapolating the research results to continuous debris flow conditions because physical model experiments were conducted amidst intermittent debris flow surges in this study.

5. Conclusions

The feedback mechanisms of bank retreat and the lateral erosion of debris flow surges were investigated in this study using five types of bank soil and multiple debris flow surges. Based on physical experiments, the following conclusions were drawn.

- The debris flow channel bank retreat process was divided into two stages. First, toe cutting was primarily
 driven by hydraulic erosion. Second, bank collapse resulted from the coupling of hydraulic erosion and
 gravity-induced toppling failure. The dominant mode of gravity erosion was toppling failure, with the frequency of such failures diminishing as the fine particle content in the bank soil increased.
- 2. The bank retreat process had a significant negative feedback loop. Bank erosion led to channel bed widening, subsequently causing a decrease in flow depth. Consequently, this reduction in flow depth mitigated bank erosion. A clear pattern was found in the intricate interplay of hydraulic erosion and toppling failure. The erosion efficiency with respect to the erosion length (ζ) exhibited a linear negative correlation with the relative bed widening width. Moreover, the mean value of ζ decreased with an increase in the fine particle content of the bank soils.
- 3. A parameterized bank retreat model was developed that considered the initial erosion efficiency with respect to erosion length (ζ_0), the maximum relative bed widening width ($b_{e,\max}^*$), channel topography (M), and debris flow volume (V_D^*). In our experiments, ζ_0 first increased and then decreased with rising fine particle content in

WANG ET AL. 13 of 17



bank soils (μ), peaking approximately 6%/m when $\mu=0.028$. The relationship between $b_{e,\max}^*$ and μ was negatively correlated and followed a power function.

Notation

A	the cross-sectional area of flow
b	the width of channel bed
B	the flow width at the free surface
b_0	the initial width of channel bed
$b_{ m e}$	the bed widening width (bank retreat distance)
$b_{ m e} ^*$	the relative bed widening width
$b_{ m i}$	the channel bed width after the <i>i</i> th debris flow surge $(i = 1, 2,, 10)$
$b_{\mathrm{e,i}}^{*}$	the relative bed widening width after the ith debris flow surge
$b_{\mathrm{e,max}}^{}*$	the maximum relative bed widening width $(b_{e,max}^* = \zeta_0/k)$
Cv	the sediment volume fraction of debris flow; D the particle size
D_{c}	describing the coarse particle content of the bank soils
Fr	the Froude numbers of debris flow
g	the gravitational acceleration
h	the flow depth of debris flow at the Cross-section 1 in Figure 1a
k	the attenuation coefficient of ζ
$L_{ m pote}$	the length of the potential bank erosion section
M	the dimensionless parameters characterizing geomorphological characteristics of the erosion section channel $(M = \tan \alpha/b_0)$
Qd	the discharge of debris flow
$S_{ m bed}$	the slope of the flume bed
v	the flow velocity of debris flow at the Cross-section 1 in Figure 1a
Vd	the volume of a debris flow surge; VD the accumulated volume of the debris flow
V_{D}^{*}	the relative accumulated volume of the debris flow $(V_D^* = V_D/b_0^3)$
$V_{ m ero}$	the cumulative bank erosion volume
α	the initial slope angle of the channel bank (Figure 9a)
$\Delta b_{ m e}$	the variation of $b_{\rm e}$
$\Delta b_{\mathrm{e}}{}^{*}$	the relative variation of b_e ($\Delta b_e^* = \Delta b_e/b_0$)
$\Delta V_{ m D}$	the variation of cumulative debris flow volume
$\Delta V_{\rm D}{}^*$	the relative variation of cumulative debris flow volume
$\varDelta V_{\mathrm{D,i}}$	the debris flow volume of the <i>i</i> th debris flow surge ($\Delta V_{\mathrm{D,i}} = V_{\mathrm{d}}$)
$\varDelta V_{\rm ero}$	the variation of bank erosion volume
$\varDelta V_{\rm ero}{}^*$	the relative variation of bank erosion volume
$\varDelta V_{\rm ero,i}$	the bank erosion volume of the ith debris flow surge

WANG ET AL. 14 of 17



the bank erosion efficiency with respect to erosion length the initial bank erosion efficiency with respect to erosion length ζ_0 $\zeta_{\rm i}$ the bank erosion efficiency with respect to erosion length of the ith debris flow surge a scaling distribution parameter characterizing the fine particle content of the bank soils (Li μ et al., 2013) the density of bank soils ρ the dry densities of bank soils $\rho_{\rm d}$ the density of the particle material $\rho_{\rm s}$ the gravimetric water contents of bank soils ω

Data Availability Statement

The study data could be accessed at https://zenodo.org/records/10868817.

Acknowledgments References

This study was supported by the National Natural Science Foundation of China (Grant 41925030) and the Second Tibetan Plateau Scientific Expedition and Research Program (2019QZKK0904). The authors thank the support from the Dongchuan Debris Flow Observation and Research Station (DDFORS), Chinese Academy of Sciences. We thank the Editor Ellen Wohl, Christophe Ancey and another Associate Editor, Colin Thorne and four anonymous reviewers for their valuable suggestions. The authors have no conflicts of interest to declare.

Alzo'ubi, A. K., Martin, C. D., & Cruden, D. M. (2010). Influence of tensile strength on toppling failure in centrifuge tests. *International Journal of Rock Mechanics and Mining Sciences*, 47(6), 974–982. https://doi.org/10.1016/j.ijrmms.2010.05.011

Bathurst, J. C., Hey, R. D., & Thorne, C. R. (1979). Secondary flow and shear stress at river bends. *Journal of the Hydraulics Division*, 105(10), 1277–1295. https://doi.org/10.1061/JYCEAJ.0005285

Berger, C., McArdell, B. W., & Schlunegger, F. (2011). Direct measurement of channel erosion by debris flows, Illgraben, Switzerland. *Journal of Geophysical Research*, 116(F1). https://doi.org/10.1029/2010JF001722

Brasington, J., Vericat, D., & Rychkov, I. (2012). Modeling river bed morphology, roughness, and surface sedimentology using high resolution terrestrial laser scanning. Water Resources Research, 48(11). https://doi.org/10.1029/2012WR012223

Brunier-Coulin, F., Cuéllar, P., & Philippe, P. (2020). Generalized Shields criterion for weakly cohesive granular materials. *Physical Review Fluids*, 5(3), 034308. https://doi.org/10.1103/PhysRevFluids.5.034308

Carson, M. A., & Kirkby, M. J. (1972). Hillslope form and process. Cambridge University Press.

Chen, D., & Tang, C. (2012). Evaluating secondary flows in the evolution of sine-generated meanders. *Geomorphology*, 163, 37–44. https://doi.org/10.1016/j.geomorph.2012.04.010

Chen, J., Chen, X., Zhao, W., & You, Y. (2018). Debris flow drainage channel with energy dissipation structures: Experimental study and engineering application. *Journal of Hydraulic Engineering*, 144(10), 06018012. https://doi.org/10.1061/(ASCE)HY.1943-7900.0001523

Chen, J. G., Liu, W. R., Zhao, W. Y., Jiang, T., Zhu, Z., & Chen, X. Q. (2021). Magnitude amplification of flash floods caused by large woody in Keze gully in Jiuzhaigou National Park, China. Geomatics. *Natural Hazards and Risk*, 12(1), 2277–2299. https://doi.org/10.1080/19475705. 2021.1961882

Chen, N. S., Yang, C. L., Zhou, W., Wei, F. Q., Li, Z. L., Han, D., & Hu, G. S. (2011). A new total volume model of debris flows with intermittent surges: Based on the observations at Jiangjia Valley, southwest China. *Natural Hazards*, 56(1), 37–57. https://doi.org/10.1007/s11069-010-9548-7

Chen, X. Q., Cui, P., You, Y., & Liu, J. (2012). Post-earthquake changes and prediction of debris flow scales in subao river valley, beichuan county, sichuan province, China. *Environmental Earth Sciences*, 65(4), 995–1003. https://doi.org/10.1007/s12665-011-0949-4

Choi, C. E., Ng, C. W. W., Au-Yeung, S. C. H., & Goodwin, G. R. (2015). Froude characteristics of both dense granular and water flows in flume modelling. Landslides, 12(6), 1197–1206. https://doi.org/10.1007/s10346-015-0628-8

Church, M., & Jakob, M. (2020). What is a debris flood? Water Resources Research, 56(8), e2020WR027144. https://doi.org/10.1029/2020WR027144

Cluer, B., & Thorne, C. (2014). A stream evolution model integrating habitat and ecosystem benefits. River Research and Applications, 30(2), 135–154. https://doi.org/10.1002/rra.2631

Cui, P., Hu, K., Zhuang, J., Yang, Y., & Zhang, J. (2011). Prediction of debris-flow danger area by combining hydrological and inundation simulation methods. *Journal of Mountain Science*, 8, 1–9. https://doi.org/10.1007/s11629-011-2040-8

Cui, P., Zeng, C., & Lei, Y. (2015). Experimental analysis on the impact force of viscous debris flow. Earth Surface Processes and Landforms, 40(12), 1644–1655. https://doi.org/10.1002/esp.3744

Cui, P., Zhou, G. G., Zhu, X. H., & Zhang, J. Q. (2013). Scale amplification of natural debris flows caused by cascading landslide dam failures. Geomorphology, 182, 173–189. https://doi.org/10.1016/j.geomorph.2012.11.009

Cui, W. R., Chen, J. G., Chen, X. Q., Tang, J. B., & Jin, K. (2023). Debris flow characteristics of the compound channels with vegetated floodplains. *Science of the Total Environment*, 868, 161586. https://doi.org/10.1016/j.scitotenv.2023.161586

Darby, S. E., Trieu, H. Q., Carling, P. A., Sarkkula, J., Koponen, J., Kummu, M., et al. (2010). A physically based model to predict hydraulic erosion of fine-grained riverbanks: The role of form roughness in limiting erosion. *Journal of Geophysical Research*, 115(F4). https://doi.org/ 10.1029/2010JF001708

Davidson, S. L., & Eaton, B. C. (2018). Beyond regime: A stochastic model of floods, bank erosion, and channel migration. Water Resources Research, 54(9), 6282–6298. https://doi.org/10.1029/2017WR022059

de Haas, T., & Woerkom, T. V. (2016). Bed scour by debris flows: Experimental investigation of effects of debris-flow composition. Earth Surface Processes and Landforms, 41(13), 1951–1966. https://doi.org/10.1002/esp.3963

WANG ET AL. 15 of 17



- Domnik, B., & Pudasaini, S. P. (2012). Full two-dimensional rapid chute flows of simple viscoplastic granular materials with a pressure-dependent dynamic slip-velocity and their numerical simulations. *Journal of Non-Newtonian Fluid Mechanics*, 173, 72–86. https://doi.org/10.1016/j.jnnfm.2012.03.001
- Du, J. H., Zhou, G. G., Tang, H., Turowski, J., & Cui, K. F. (2023). Classification of stream, hyperconcentrated, and debris flow using dimensional analysis and machine learning. *Water Resources Research*, 59(2). https://doi.org/10.1029/2022WR033242
- Dunne, K. B., & Jerolmack, D. J. (2020). What sets river width? Science Advances, 6(41), eabc1505. https://doi.org/10.1126/sciadv.abc1505
- Fan, R. L., Zhang, L. M., Wang, H. J., & Fan, X. M. (2018). Evolution of debris flow activities in Gaojiagou Ravine during 2008–2016 after the Wenchuan earthquake. *Engineering Geology*, 235, 1–10. https://doi.org/10.1016/j.enggeo.2018.01.017
- French, R. H. (1985). Open-channel hydraulics. McGraw-Hill.
- Garcia-Martinez, R., & Lopez, J. L. (2005). Debrisflow of december 1999 in Venezuela. In M. Jakob & O. Hungr (Eds.), Debris-flow hazardsand related phenomena. *Praxis* (pp. 519–538). Springe.
- Gong, Z., Zhao, K., Zhang, C., Dai, W., Coco, G., & Zhou, Z. (2018). The role of bank collapse on tidal creek ontogeny: A novel process-based model for bank retreat. *Geomorphology*, 311, 13–26. https://doi.org/10.1016/j.geomorph.2018.03.016
- Guo, X., Li, Y., Cui, P., Yan, H., & Zhuang, J. (2020). Intermittent viscous debris flow formation in Jiangjia Gully from the perspectives of hydrological processes and material supply. *Journal of Hydrology*, 589, 125184. https://doi.org/10.1016/j.jhydrol.2020.125184
- Hu, K. H., Cui, P., & Zhang, J. Q. (2012). Characteristics of damage to buildings by debris flows on 7 August 2010 in Zhouqu, Western China. Natural Hazards and Earth System Sciences, 12(7), 2209–2217. https://doi.org/10.5194/nhess-12-2209-2012
- Huebl, J., & Kaitna, R. (2021). Monitoring debris-flow surges and triggering rainfall at the Lattenbach Creek, Austria. Environmental and Engineering Geoscience, 27(2), 213–220. https://doi.org/10.2113/EEG-D-20-00010
- Hungr, O. (2005). Classification and terminology. edited by. In M. Jakob & O. Hungr (Eds.), *Debris-flow hazards and related phenomena* (pp. 9–23).
- Imaizumi, F., Masui, T., Yokota, Y., Tsunetaka, H., Hayakawa, Y., & Hotta, N. (2019). Initiation and runout characteristics of debris flow surges in Ohya landslide scar, Japan. Geomorphology, 339(5), 58–69. https://doi.org/10.1016/j.geomorph.2019.04.026
- Iverson, R. M. (1997). The physics of debris flows. Reviews of Geophysics, 35(3), 245-296. https://doi.org/10.1029/97RG00426
- Iverson, R. M. (2012). Elementary theory of bed-sediment entrainment by debris flows and avalanches. *Journal of Geophysical Research*, 117(F3), F03006. https://doi.org/10.1029/2011JF002189
- Iverson, R. M. (2015). Scaling and design of landslide and debris-flow experiments. Geomorphology, 244, 9–20. https://doi.org/10.1016/j.geomorph.2015.02.033
- Kean, J. W., McCoy, S. W., Tucker, G. E., Staley, D. M., & Coe, J. A. (2013). Runoff-generated debris flows: Observations and modeling of surge initiation, magnitude, and frequency. *Journal of Geophysical Research: Earth Surface*, 118(4), 2190–2207. https://doi.org/10.1002/jgrf.20148
- Kim, D., Sagong, M., & Lee, Y. (2005). Effects of fine aggregate content on the mechanical properties of the compacted decomposed granitic soils. *Construction and Building Materials*, 19(3), 189–196. https://doi.org/10.1016/j.conbuildmat.2004.06.002
- Kouakou, N. M., Cuisinier, O., & Masrouri, F. (2020). Estimation of the shear strength of coarse-grained soils with fine particles. Transportation Geotechnics, 25, 100407. https://doi.org/10.1016/j.trgeo.2020.100407
- Lancaster, S. T., Hayes, S. K., & Grant, G. E. (2003). Effects of wood on debris flow runout in small mountain watersheds. *Water Resources Research*, 39(6). https://doi.org/10.1029/2001WR001227
- Lapillonne, S., Fontaine, F., Liebault, F., Richefeu, V., & Piton, G. (2023). Debris-flow surges of a very active alpine torrent: A field database. Natural Hazards and Earth System Sciences, 23(4), 1241–1256. https://doi.org/10.5194/nhess-23-1241-2023
- Li, S., You, Y., Chen, X., Liu, J., & Chen, J. (2019). Regulation effectiveness of a window-check dam on debris flows. *Engineering Geology*, 253, 205–213. https://doi.org/10.1016/j.enggeo.2019.03.020
- Li, Y., Huang, C., Wang, B., Tian, X., & Liu, J. (2017). A unified expression for grain size distribution of soils. *Geoderma*, 288, 105–119. https://doi.org/10.1016/j.geoderma.2016.11.011
- Li, Y., Zhou, X., Su, P., Kong, Y., & Liu, J. (2013). A scaling distribution for grain composition of debris flow. *Geomorphology*, 192, 30–42. https://doi.org/10.1016/j.geomorph.2013.03.015
- Lyu, L., Wang, Z., Cui, P., & Xu, M. (2017). The role of bank erosion on the initiation and motion of gully debris flows. *Geomorphology*, 285, 137–151. https://doi.org/10.1016/j.geomorph.2017.02.008
- Lyu, L., Xu, M., Wang, Z., Cui, Y., & Blanckaert, K. (2022). A field investigation on debris flows in the incised Tongde sedimentary basin on the northeastern edge of the Tibetan Plateau. Catena, 208, 105727. https://doi.org/10.1016/j.catena.2021.105727
- MacKenzie, L. G., & Eaton, B. C. (2017). Large grains matter: Contrasting bed stability and morphodynamics during two nearly identical experiments. Earth Surface Processes and Landforms, 42(8), 1287–1295. https://doi.org/10.1002/esp.4122
- Mergili, M., Pudasaini, S. P., Emmer, A., Fischer, J. T., Cochachin, A., & Frey, H. (2020). Reconstruction of the 1941 GLOF process chain at lake palcacocha (cordillera blanca, Peru). Hydrology and Earth System Sciences, 24(1), 93–114. https://doi.org/10.5194/hess-24-93-2020
- Nagl, G., Hübl, J., & Scheidl, C. (2024). Real-scale measurements of debris-flow run-ups. *Landslides*, 21(5), 963–973. https://doi.org/10.1007/s10346-023-02204-6
- Osman, A. M., & Thorne, C. R. (1988). Riverbank stability analysis. I: Theory. *Journal of Hydraulic Engineering*, 114(2), 134–150. https://doi.org/10.1061/(ASCE)0733-9429(1988)114:2(134)
- Ouyang, C. J., Wang, Z., An, H., Liu, X., & Wang, D. (2019). An example of a hazard and risk assessment for debris flows—A case study of niwan gully, wudu, China. *Engineering Geology*, 263, 105351. https://doi.org/10.1016/j.enggeo.2019.105351
- Parker, G., Shimizu, Y., Wilkerson, G. V., Eke, E. C., Abad, J. D., Lauer, J. W., et al. (2011). A new framework for modeling the migration of meandering rivers. Earth Surface Processes and Landforms, 36(1), 70–86. https://doi.org/10.1002/esp.2113
- Pudasaini, S. P., & Domnik, B. (2009). Energy considerations in accelerating rapid shear granular flows. *Nonlinear Processes in Geophysics*, 16(3), 399–407. https://doi.org/10.5194/npg-16-399-2009
- Pudasaini, S. P., & Fischer, J. T. (2020). A mechanical erosion model for two-phase mass flows. *International Journal of Multiphase Flow*, 132, 103416. https://doi.org/10.1016/j.ijmultiphaseflow.2020.103416
- Pudasaini, S. P., & Krautblatter, M. (2021). The mechanics of landslide mobility with erosion. *Nature Communications*, 12(1), 6793. https://doi.org/10.1038/s41467-021-26959-5
- Pudasaini, S. P., & Mergili, M. (2019). A multi-phase mass flow model. Journal of Geophysical Research: Earth Surface, 124(12), 2920–2942. https://doi.org/10.1029/2019JF005204
- Rickenmann, D. (1999). Empirical relationships for debris flows. Natural Hazards, 19(1), 47-77. https://doi.org/10.1023/A:1008064220727
- Ruan, H., Chen, H., Li, Y., Chen, J., & Li, H. (2021). Study on the downcutting rate of a debris flow dam based on grain-size distribution. Geomorphology, 391, 107891. https://doi.org/10.1016/j.geomorph.2021.107891

WANG ET AL. 16 of 17



- Sawaske, S. R., & Freyberg, D. L. (2012). A comparison of past small dam removals in highly sediment-impacted systems in the U.S. Geomorphology, 151–152, 50–58. https://doi.org/10.1016/j.geomorph.2012.01.013
- Schwab, M., Rieke-Zapp, D., Schneider, H., Liniger, M., & Schlunegger, F. (2008). Landsliding and sediment flux in the central Swiss alps: A photogrammetric study of the schimbrig landslide, entlebuch. *Geomorphology*, 97(3–4), 392–406. https://doi.org/10.1016/j.geomorph.2007. 08.019
- Song, P., & Choi, C. E. (2021). Revealing the importance of capillary and collisional stresses on soil bed erosion induced by debris flows. *Journal of Geophysical Research: Earth Surface*, 126(5), e2020JF005930. https://doi.org/10.1029/2020JF005930
- Stecca, G., Measures, R., & Hicks, D. M. (2017). A framework for the analysis of noncohesive bank erosion algorithms in morphodynamic modeling. Water Resources Research, 53(8), 6663–6686. https://doi.org/10.1002/2017WR020756
- Takahashi, T. (2007). Debris flow: Mechanics, prediction and countermeasures. Taylor and Francis Ltd.
- Thorne, C. R. (1978). Processes of bank erosion in river channels. UEA doctoral thesis.
- Thorne, C. R. (1982). In R. D. Hey, J. C. Bathurst, & C. R. Thorne (Eds.), *Processes and mechanisms of river bank erosion: Chapter 9, in Gravel bed Rivers.* Wiley.
- Thorne, C. R., & Tovey, N. K. (1981). Stability of composite river banks. Earth Surface Processes and Landforms, 6(5), 469–484. https://doi.org/10.1002/esp.3290060507
- van Dijk, W. M., Teske, R., Vande Lageweg, W. I., & Kleinhans, M. G. (2013). Effects of vegetation distribution on experimental river channel dynamics. Water Resources Research, 49(11), 7558–7574. https://doi.org/10.1002/2013wr013574
- Wang, X., Chen, J., Chen, X., Chen, H., Zhao, W., Ruan, H., & Wang, J. (2024). Bank erosion process and distribution along channel caused by multiple debris flow surges. [Dataset]. https://doi.org/10.5281/zenodo.10868817. Zenodo.
- Wang, X. A., Chen, J. G., Chen, H. Y., Chen, X. Q., Li, S., & Zhao, W. Y. (2022). Erosion process of multiple debris flow surges caused by check dam removal: An experimental study. Water Resources Research, 58(3), e2021WR030688. https://doi.org/10.1029/2021WR030688
- Wolman, M. G., & Miller, J. P. (1960). Magnitude and frequency of forces in geomorphic processes. The Journal of Geology, 68(1), 54–74. https://doi.org/10.1086/626637
- Wu, W., Perera, C., Smith, J., & Sanchez, A. (2018). Critical shear stress for erosion of sand and mud mixtures. *Journal of Hydraulic Research*, 56(1), 96–110. https://doi.org/10.1080/00221686.2017.1300195
- Yang, C. J., Jen, C. H., Cheng, Y. C., & Lin, J. C. (2021). Quantification of mudcracks-driven erosion using terrestrial laser scanning in laboratory runoff experiment. *Geomorphology*, 375, 107527. https://doi.org/10.1016/j.geomorph.2020.107527
- Yao, P., Su, M., Wang, Z., van Rijn, L. C., Stive, M. J., Xu, C., & Chen, Y. (2022). Erosion behavior of sand-silt mixtures: Revisiting the erosion threshold. Water Resources Research, 58(9), e2021WR031788. https://doi.org/10.1029/2021WR031788
- Yu, B., & Wolman, M. G. (1987). Some dynamic aspects of river geometry. Water Resources Research, 23(3), 501–509. https://doi.org/10.1029/ WR023i003p00501
- WROZSHOSPOOSOT
 Zanuttigh, B., & Lamberti, A. (2007). Instability and surge development in debris flows. Reviews of Geophysics, 45(3). https://doi.org/10.1029/2005RG000175
- Zhang, J., Luo, D., Li, H., Pei, L., & Yao, Q. (2023). Experimental study on gully erosion characteristics of mountain torrent debris flow in a strong earthquake area. Water, 15(2), 283. https://doi.org/10.3390/w15020283
- Zhang, K., Gong, Z., Zhao, K., Wang, K., Pan, S., & Coco, G. (2021). Experimental and numerical modeling of overhanging riverbank stability. Journal of Geophysical Research: Earth Surface, 126(10), e2021JF006109. https://doi.org/10.1029/2021JF006109
- Zhang, S., & Zhang, L. M. (2017). Impact of the 2008 Wenchuan earthquake in China on subsequent long-term debris flow activities in the epicentral area. *Geomorphology*, 276, 86–103. https://doi.org/10.1016/j.geomorph.2016.10.009
- Zhao, K., Coco, G., Gong, Z., Darby, S. E., Lanzoni, S., Xu, F., et al. (2022). A review on bank retreat: Mechanisms, observations, and modeling. *Reviews of Geophysics*, 60(2), e2021RG000761. https://doi.org/10.1029/2021RG000761
- Zhao, K., Gong, Z., Xu, F., Zhou, Z., Zhang, C. K., Perillo, G. M. E., & Coco, G. (2019). The role of collapsed bank soil on tidal channel evolution:
 A process-based model involving bank collapse and sediment dynamics. *Water Resources Research*, 55(11), 9051–9071. https://doi.org/10.1029/2019WR025514
- Zhao, K., Gong, Z., Zhang, K., Wang, K., Chuang, J. C., Zhou, Z., et al. (2020). Laboratory experiments of bank collapse: The role of bank height and near-bank water depth. *Journal of Geophysical Research: Earth Surface*, 125(5), e2019JF005281. https://doi.org/10.1029/2019JF005281
- Zhou, G. G., Cui, P., Tang, J. B., Chen, H. Y., Zou, Q., & Sun, Q. C. (2015). Experimental study on the triggering mechanisms and kinematic properties of large debris flows in Wenjia Gully. *Engineering Geology*, 194, 52–61. https://doi.org/10.1016/j.enggeo.2014.10.021
- Zhou, G. G. D., Hu, H. S., Song, D., Zhao, T., & Chen, X. Q. (2019). Experimental study on the regulation function of slit dam against debris flows. *Landslides*, 16(1), 75–90. https://doi.org/10.1007/s10346-018-1065-2

WANG ET AL. 17 of 17